Numerical Investigation of a 3-D Flow Past an Impenetrable Rotating Microparticle at Low and Moderate Reynolds Numbers

M.R. Meigounpoory[1] and GH. Atefi[2]
Mech. Eng. Dep't.
Iran Univ. of science & Tech.

H. Niazmand[3]
Mech. Eng. Dep't.
Mashad Ferdowsi Univ.

A. Mirbozorgi[4]
Mech. Eng. Dep't.
Birjand Univ.

ABSTRACT
Computations are performed to determine the steady 3-D viscous fluid flow forces acting on an impenetrable rotating spherical suspended particle at low and moderate Reynolds numbers in the range of $0.1 \le Re \le 100$. In order to extend the capabilities of the finite volume method, the boundary (body) fitted coordinates (BFC) method is used. Transformation of the governing partial differential equation to algebraic relations is based on the finite volume method and collocated variables arrangement. For solving the algebraic relations, the TDMA in a periodic state is used. To approximate the convective fluxes, the differencing scheme of Van Leer is used and the SIMPLEC algorithm handles the linkage between velocity and the pressure. Rotation increases the drag and lift forces exerted by flow at the surface of on the sphere. Using velocity components in Cartesian coordinates causes slight decrease in the run time of program with respect to using it in contra-variant and covariant coordinates. The flow patterns are changed with increasing rotation at x-y plane, but flow at x-y plane remains symmetric the present numerical results are in complete accord with other results of flow around a rotating sphere.

Key Words: Rotating Suspended Particle, 3-D Flow, Body Fitted Coordinate

بررسی عددی جریان کاملاً سه بعدی حول یک میکرو ذره کروی چرخان درمحدوده اعدادرینولدز متوسط و پایین

محمدرضا میگون پوری[1] و غلامعلی عاطفی[2]
دانشکده مهندسی مکانیک
دانشگاه علم وصنعت ایران

حمید نیازمند[3]
دانشکده مهندسی مکانیک
دانشگاه فردوسی مشهد

علی میر بزرگی[4]
دانشکده مهندسی مکانیک
دانشگاه بیرجند

چکیده
در این مقاله به بررسی عددی جریان سه بعدی سیال غیرقابل تراکم در اطراف یک ذره کروی‌جامد معلق در حال دوران درمحدوده $0.1 \le Re \le 100$ پرداخته می شود. به این منظور یک کد عددی سه بعدی نوشته شده که برای گسسته سازی معادلات دیفرانسیل جزئی با روش جبری از روش حجم محدود و با آرایش مرتب شده متغیرها و برای مدل نمودن شارهای جابجایی از روش ون لیر و برای ارتباط دادن میدانهای فشار وسرعت از روش سیمپل سی استفاده می کند. برای افزایش قابلیت های روش حجم محدود، از روش مختصات منطبق بر مرز استفاده می شود و سیستم معادلات جبری توسط الگوریتم TDMA حل می‌گردد. در این مقاله مشخص شد که چرخش کره باعث تغییرات زیادی در الگوی جریان و توزیع فشار و ورتیسیتی جریان حول آن می‌شود. در اعداد رینولدز پایین، چرخش ذره کروی تاثیر زیادی بر ضرایب درگ ولیفت ندارد ولی در اعداد رینولدز بالاتر تاثیرچرخش برمقادیر ضرایب برا وپسا افزایش می یابد. همچنین، به کارگیری مولفه های کارتزین سرعت به جای مولفه های کووارینت و کونتراوارینت باعث کاهش قابل ملاحظه حجم محاسبات می شود. مقایسه نتایج حاصله با نتایج سایر محققین صحت روند حل والگوریتم های مورد استفاده را تایید می کند.

واژه های کلیدی: کره چرخان، تحلیل سه بعدی جریان، مختصات منطبق بر مرز

1-PhD Student(Corresponding Author): mr_meigoonpoory@mail.iust.ac.ir
2-Associate Professor: Atefi@ iust.ac.ir
3-Assistant Professor
4-Assistant Professor

Symbols and Abbreviations

A	Area
D	Diameter of Sphere
L	Wake Length
$\vec{n}$	Normal Unit Vector
p	Pressure
r, θ, φ	Spherical Coordinates
R	Radius of Sphere
Re	Reynolds Number, $Re = U_\infty D/\nu$
t	Time
u, v, w	Velocity Components in the x, y, z Directions
U_∞	Free Stream Velocity
$\vec{V}$	Velocity Vector
C_D	Drag Coefficient
C_{Ly}	Lift Coefficient in y Direction
ν	Kinematic Viscosity
θ_s	Separation Angle
τ	Non-Dimensional Time, $\tau = tU_\infty/D$
$\vec{\vec{\tau}}$	Viscous Stress Tensor
f	Fluid
∞	Free-Stream

Introduction

Flow over spheres is a fundamental problem encountered in many engineering problems. It is well known that the motion of spherical particles have many applications in industries, such as hydrodynamic dispersion in quiescent sedimenting suspensions, the dynamics of bubbles and drop or particle in arbitrary motion at different Reynolds numbers, Sedimentation of noncolloidal Particles, osmotic phenomena, transport of groundwater colloids, and the permeability reduction due to migrating fines in enhanced oil recovery and hydrodynamic dispersion, the motion of fuel droplets in combustors, solid particle in air, and two phase flows, like motion spherical bubbles and droplets in fluid flow, solid particle in air. It is well known that the motion of spherical particles in some applications also involves no-slip condition such as the motion of fuel droplets in combustors, solid particle in air, and some other motion of spherical particles such as bubbles involves slip condition on the surface.

Although particle rotation typically occurs around an arbitrary axis in space, investigation of cases with rotation axes normal and parallel to the principal flow direction can provide fundamental information. The characteristics of the flow field for particle rotation in the stream wise direction (*spin*) are quite different from that in the transverse direction (*rotation*). Rotation displaces and reduces the recirculation region of the wake such that at sufficiently high rotational speeds it is completely suppressed [1], while spin has the opposite effect. The structure of flow at the near wake region has a strong influence on the behavior of the drag and lifts forces as well as the other characteristics of the particle, and therefore, deserves close examination. For uniform flow past a sphere, the wake forms at $Re \cong 20$ and undergoes several well-defined transitions as the Reynolds number is increased. First transition occurs at $Re \cong 212$, where the axisymmetric steady wake becomes planar-symmetric yet steady and attached. In the second transition, the steady planar-symmetric wake becomes unsteady at $Re \cong 270$ forming a periodic wake with vortex shedding. The details of the wake structure in each wake regime have been investigated both experimentally and theoretically [2-8]. However, a review of the relevant literature provides limited information on the effects of particle spin and rotation. The case of particle rotation has attracted some attention in the literature, where the experimental studies of Best [1] and Brakla and Auchterlonie [9], Oesterle and Dinh [10], and the numerical studies of Salem and Oesterle [11], and Kurose and Komori [12] can be mentioned among others. However, for the case of a spinning sphere much less information is available in this *Re* range. The only known work is the numerical study of Kim and Choi [13]. They considered $Re = 100$ in the steady symmetrical regime, $Re = 250$ in the steady non-symmetrical regime, and $Re = 300$ in the unsteady wake regime, for angular velocities of $\Omega_x \leq 1$. It is reported that the forces acting on the sphere are influenced by spin, and the vortical structures behind the particle are significantly modified. For higher *Re* flows over spinning spheres, Clift et al. [14] have summarized previous studies and pointed out that the transition to turbulence, which is identified by a sudden drop in the standard drag curve, occurs at lower *Re* with increased spin. Similar behavior is observed in the present study at moderate *Re*, such that increasing particle spin reduces the transitional *Re* between the different wake regimes. Niazmand and Renksizbulut [15] and [16] carried out numerical investigations of the flow and temperature fields around rotating spheres with surface blowing. It is shown that transient behavior of important flow parameters such as the lift and drag coefficients are significantly influenced by particle rotation and surface blowing. However, the surface-averaged heat transfer rates are not influenced appreciably by particle rotation even at high rotational speeds, whereas the local heat transfer rates are drastically affected. Literature review shows that the lack of study about flow around the rotating sphere at moderate Reynolds numbers. Recently, Numerical analysis of 3D flow past a stationary sphere with

slip condition at low and moderate Reynolds numbers has been investigated by Atefi et al [17].

The aim of the present study is to examine the flow field around a rotating sphere numerically. The range of Reynolds numbers considered here are 1 to 100, and the dimensionless angular velocity will be varied up to 1. The combined effects of particle Reynolds number and rotation will also be addressed. Important features of the flow properties will be compared to their counterparts for rotating spheres reported in literature review.

3. Problem Formulation

The flow geometry and sphere in generalized coordinates (ξ,η,ζ), which in the present problem lie along the spherical coordinates (θ,φ,r) respectively, are shown in Fig. **1**.

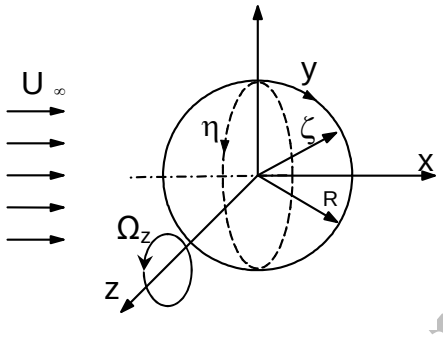

Figure (1): Flow geometry and coordinates.

A uniform stream in the positive *x*-direction flows over a sphere rotating with constant angular velocity ω_z around the principal flow axis. The laminar, constant-property, viscous flow under study is governed by the usual set of continuity and momentum equations as follows:

$$\vec{\nabla}.\vec{V} = 0, \qquad (1)$$

$$\frac{\partial \vec{V}}{\partial t} + \vec{V}.(\vec{\nabla}.\vec{V}) = \vec{F} - \frac{1}{\rho}\vec{\nabla}P + \nu\Delta\vec{V}, \qquad (2)$$

where ρ, $\vec{V}$ are density and velocity vector, υ kinematic viscosity and P is pressure. Inflow boundary conditions are simply $u = 1$ and v=w=0. On the surface of a solid sphere, the flow satisfies the no-slip boundary condition. For outflow, zero-gradients along the streamlines are applied for $\theta \geq 120^{\circ}$ to all variables such that:

$$\vec{V}.\vec{\nabla}f = 0, \qquad (3)$$

where, $f = u,v,w$. On the surface of a sphere, rotation with a non-dimensional angular velocity of $\Omega = R\omega_z/U_\infty$ around the *z*-axis in the counterclockwise direction, the velocity components are:

$$u = R\omega_z \cos\varphi \sin\theta/U_\infty,$$
$$v = R\omega_z \cos\varphi \cos\theta/U_\infty, \qquad (4)$$
$$w = 0,$$

where, $\vec{e}_x$, $\vec{e}_y$ and $\vec{e}_z$ are unit vectors in the *x*, *y* and *z* directions, respectively. Initial conditions correspond to a sudden introduction of a rotating sphere into an otherwise uniform free stream. The initial pressure is specified as zero over the whole computational domain. The resultant force acting on the particle is obtained by integrating the normal and tangential stresses on the sphere surface, as:

$$\vec{F} = -\int_A P.\vec{n}dA + \int_A \vec{\tau}.\vec{n}dA, \qquad (5)$$

where,

$$F_L = F_{LP} + F_{Lf} = -\int_A P\vec{e}_y.\vec{n}dA + \int_A \vec{n}.\tau.\vec{e}_y dA, \qquad (6)$$

$$F_D = F_{DP} + F_{Df} = -\int_A P\vec{e}_x.\vec{n}dA + \int_A \vec{n}.\tau.\vec{e}_x dA. \qquad (7)$$

Here, $\vec{e}_x$,$\vec{e}_y$ are unit vectors in x and y axes. which are non-dimensionalized as $\vec{C}_F = \vec{F}/(\pi R^2 \rho U_\infty^2/2)$.

The component of $\vec{C}_F$ along the *x*-axis is the drag coefficient C_D. For flow over a rotating sphere the components of $\vec{C}_F$ along the *y* axes have finite values, and therefore, the lift coefficient is defined as C_L .The drag and lift coefficient are defined as:

$$C_D = F_D/0.5\rho U_\infty^2 A \quad , \quad C_L = F_L/0.5\rho U_\infty^2 A \qquad (8)$$

4-Numerical Solution Method

The governing equations given above were solved numerically using a finite-volume method with collocated variables in a generalized 3-D coordinate system. To avoid the checker board affect, the interpolation of Rhei-chow [18] was used in the calculation of convecting mass flow rate. In order to approximate the values of convected quantities at location of each faces, the differenceing scheme of Van-Leer was used at Re=100. The scheme of SIMPLEC handles the likage between velocities and pressure fields. The resulting algebric system of equations was solved using a line-by-line iterative method with TDMA.

More detailes of the numerical method has been described in detail by Farhanieh [18] and further improved by authors to properly capture the numerical analysis of flow around of sphere at moderate Reynolds numbers.

5-Computational parameter and Numerical Accuracy

We study flow around of sphere in the range of 0.1<Re<100. Transport mechanism of fluid properties at Re=100 is convection mechanism and we use van Leer method for solving numerical problem. The accuracy of numerical algorithm was tested by predicting the axisymmetric flow around a stationary solid sphere at Re=100. we examined effects of grid resolution on drag coefficient, separation angle and dimensionless wake length of flow at Re=100. The details of the grid independence study, as well as evidence of accuracy in predicting wake features, fluid forces and in the range of parameters considered here are given elsewhere [21].

The flow is axisymmetric in this case and three dimentional solution sheme is fully exercised in a time accurate manner for all cases. As shown in Fig. **2** for most cases considered here, a numerical grid of $(\xi_{\max},\eta_{\max},\zeta_{\max})=(62,52,62)$ has been used, and the far-field boundary has been set at 10 radii from the center of the sphere. Fig. **2**. shows Coordinates, flow geometry and mesh generation around of sphere.

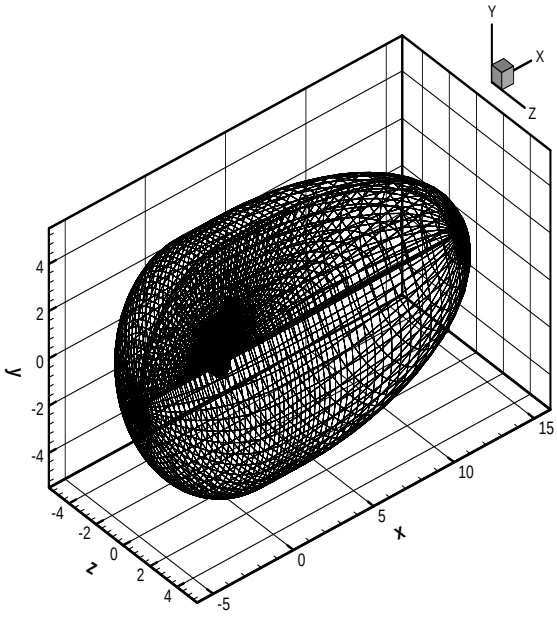

Figure (2): Coordinates , flow geometry and mesh around a sphere.

Table **1** lists the drag coefficient as a function of Reynolds number and compare them experimental results of Roos and Willmarth [3] and numerical data presented by Clift et al. [14]. The table also includes the separation angle, measured from front stagnation point, which are in good agreement with results from Clift et al. [14]. As shown in Fig. 3, the separation angle is measured from the rear stagnation point by present method with Ω_z=0 and they have compared with other numerical and analytical results.

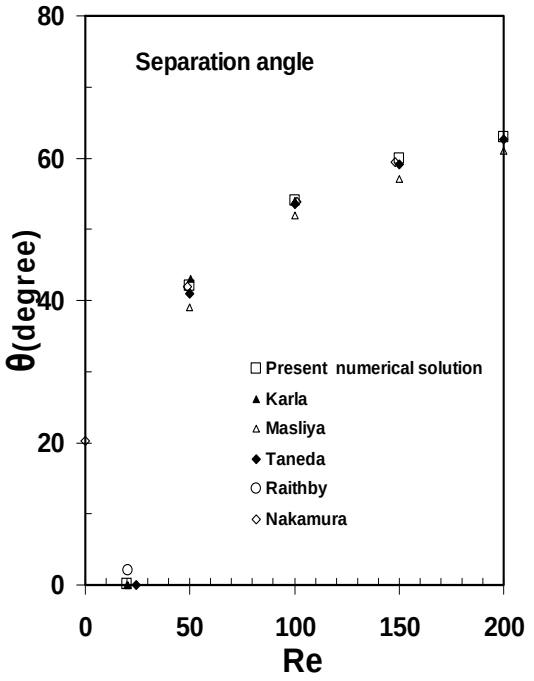

Figure (3): Comparison of separation angle for flow over an impenetrable stationary sphere.

The comparison is made with numerical results of Nakamura [4], Raithby[18], Masliya [14] and experiment results of Taneda [1] and Karla and Uhlherr[20].

Table 2 shows grid independency of flow around the rotating sphere at Re=100 and Ω_z=0.5 for different grid densities. As shown in table **2** the effect of grid resolution on drag and lift coefficient of flow at Re=100 and different outer boundary was investigated. The extend of grid expansion in some cases was adjusted based on the number of grid points and the location of the outer boundary to achieve a comparable grid density near the surface of the sphere. The maximum difference between drag coefficient between all case is about 3%.

Table (1): Comparison of our drag coefficient and separation angle with those of Clift et al. [14] and Roos & Willmarth [3] for flow over a solid sphere.

Drag Coefficient				Separation angle (θ)[a]	
Re	Present work	Roos& Willmarth [b] [3]	Clift et al [14]	Present work	Clift et al [14]
1	27.327046	-	27.315	0	0
50	1.588	1.620	1.57	139.3	139.3
100	1.095	1.090	1.096	126.8	126.5
a values of separation angle measured from the front stagnation point					
b interpolated values are use					

Table (2): Drag and lift coefficients as functions of grid density at Re=100 and at Ω_z=0.5**.**

R_∞ / R	$\xi_{\max} \times \eta_{ma} \times \zeta_{ma}$	Radial expansion factor	Lift coefficient	Drag coefficient
10	51×50×51	1.09	·0.073361	1.176802
10	51×50×61	1.09	0.073466	1.177260
10	61×50×61	1.05	0.073201	1.173813
10	71×50×71	1.04	0.073265	1.171703
20	71×50×71	1.04	0.073228	1.172564
30	81×50×81	1.04	0.0733459	1.173680

It is Clear that changing the location of the outer boundary from 10 to 20 radii and to 30 radii does not introduce considerable changes to the drag coefficient. The grid points are expanded only in the radial direction with an expansion ratio of about 1.04 at Re=100. A dimensionless time step $\Delta\tau = 0.0025$ based on diffusion time scale ($\tau_{dif} = {\nu t}/{D^2}$, where ν is kinematic viscosity and t is time) were used to initiate the calculation. It should be note that, in this analysis, the spherical particle does not accelerate owing to aerodynamic forces acting on it from the flow field.

6-Results and Discussion

Simulations are performed in the range 0.1<Re<100 covering the Two different flow regimes of classical flow past a stationary solid sphere: (I) steady attached flow for $Re \le 20$, (II) steady axisymmetric flow with separation for 20<Re<100, The effects of particle rotation will be considered for *Re* < 100, as representative of each flow regime. Transient behavior of the lift, drag will be presented for rotation in the range $\Omega_z \le 1$. Computations at different Reynolds number regimes in combination with particle rotation will also be discussed. For most cases considered here, a numerical grid of $(\xi_{\max}, \eta_{\max}, \zeta_{\max}) = (62,52,62)$ has been used, and the far-field boundary has been set at 10 radii from the center of the sphere. The grid points are expanded only in the radial direction with an expansion ratio of about 1.04 and a dimensionless time step of $\Delta\tau = 0.0025$ is used to initiate the calculations. However, this time step is increased by a factor of 1.02 to a maximum value in the range of $0.01 \le \Delta\tau_{\max} \le 0.05$ depending on the Reynolds number and rotation speed.

Present calculations are confirmed that up to *Re* ≅ 20, uniform flow past a motionless sphere does not separate despite the pressure asymmetry around the particle. Particle rotation enhances this asymmetry. If dimensionless angular velocity is increased present calculations at different Ω_z and Reynolds indicate the onset of variation in Pressure coefficient and vortisity distribution, and other flow characteristics on the surface of sphere and dispersion of flow properties in flow around a spherical particle. As shown in Fig. **4**, there is a symmetric wake region at the back of the sphere at Re=100 and Ω_z =0 in x-y plane that is perpendicular to rotating axes (z).

Global views of the effects of rotation and Reynolds number on the flow structure at Re=100 are presented in Fig. **4**. The streamlines pass through the same grid points in the flow field around the front stagnation point at different angular velocity. As expected at presence of rotation, the streamlines passing on the rotating sphere will not remain symmetric. Flow over a sphere at Re=100, Ω_z =0 forms a closed-bubble with recirculating wake of length *L* = 0.87*D*, which separates at $\theta_s = 127^\circ$. Particle rotation forms an asymmetric wake with a smaller size and sooner flow separation in x-y plane.

Two forces are exerted in the flow field around of rotating spherical particle, and they are momentums of flow and force created by rotation of sphere. When dimensionless angular velocity increases, the shear stress force exerted by rotating

effects is increased with respect to inertia force and flow tends to move in rotating direction. Increasing Ω_z >0.5 causes the growth of rotational force whereas at the regions near the spherical surface flow rotates completely around the sphere.

Fig. **5** shows the flow patterns of flow around the rotating sphere in x-z plane at Re=100 and different angular velocity. The streamlines of flow around the rotating sphere at Re=100 and x-z plane is symmetric. The wake length and separation angle decreases with increasing Ω_z angular velocity of rotating sphere. The physical reason of this behavior is related to increasing the velocity gradient near the spherical surface. Increasing angular velocity increases shear stress on the particle surface and flow sense sphere presence on the flow field more than before.

Increasing rotating number Ω_z is more profound at higher rotation. Present calculations indicate the wake length becomes smaller with increasing Ω_z until it will be disappeared at $\Omega_z \geq 0.5$.

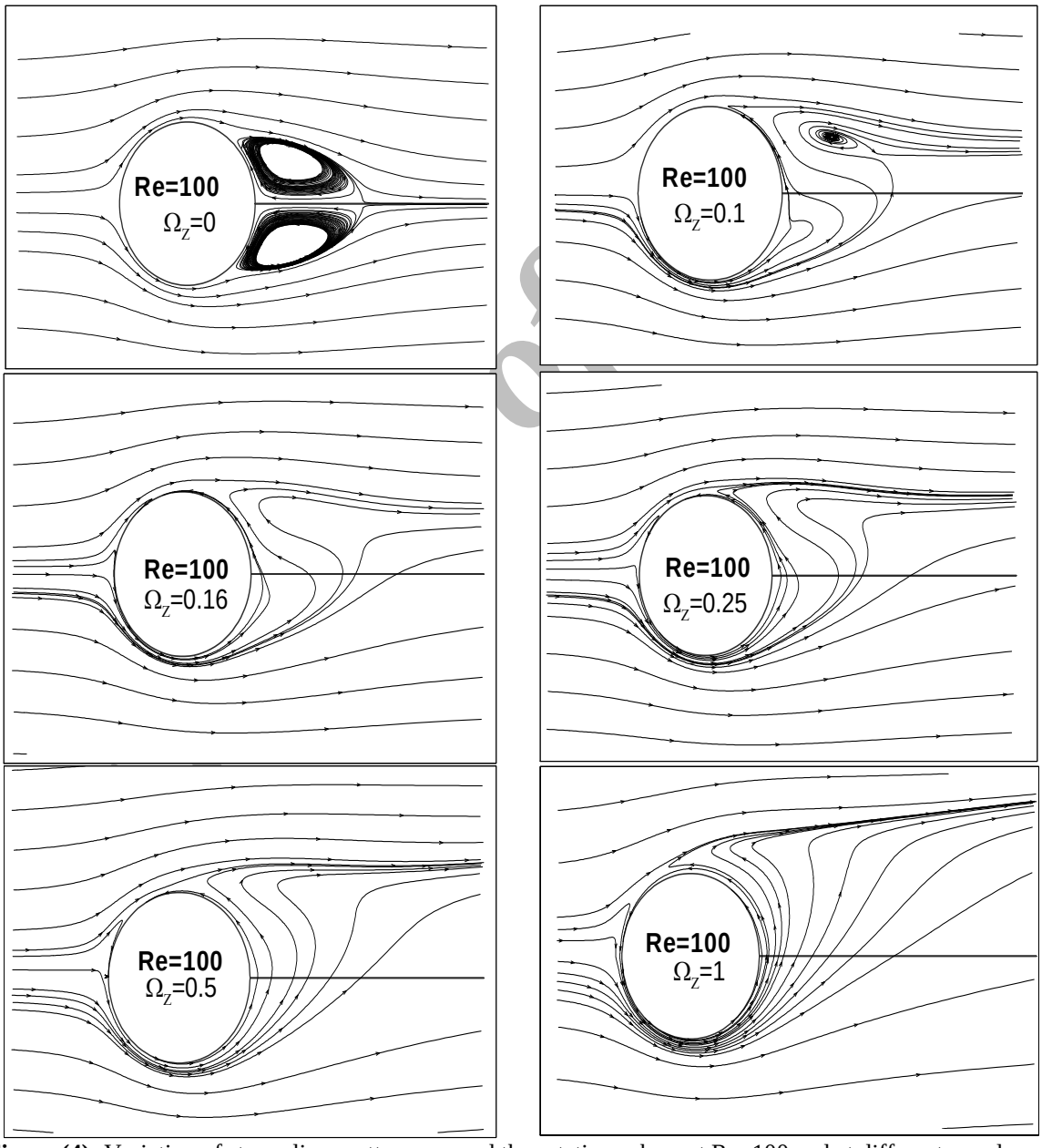

Figure (4): Variation of streamlines patterns around the rotating sphere at Re=100 and at different angular velocity in x-y plane.

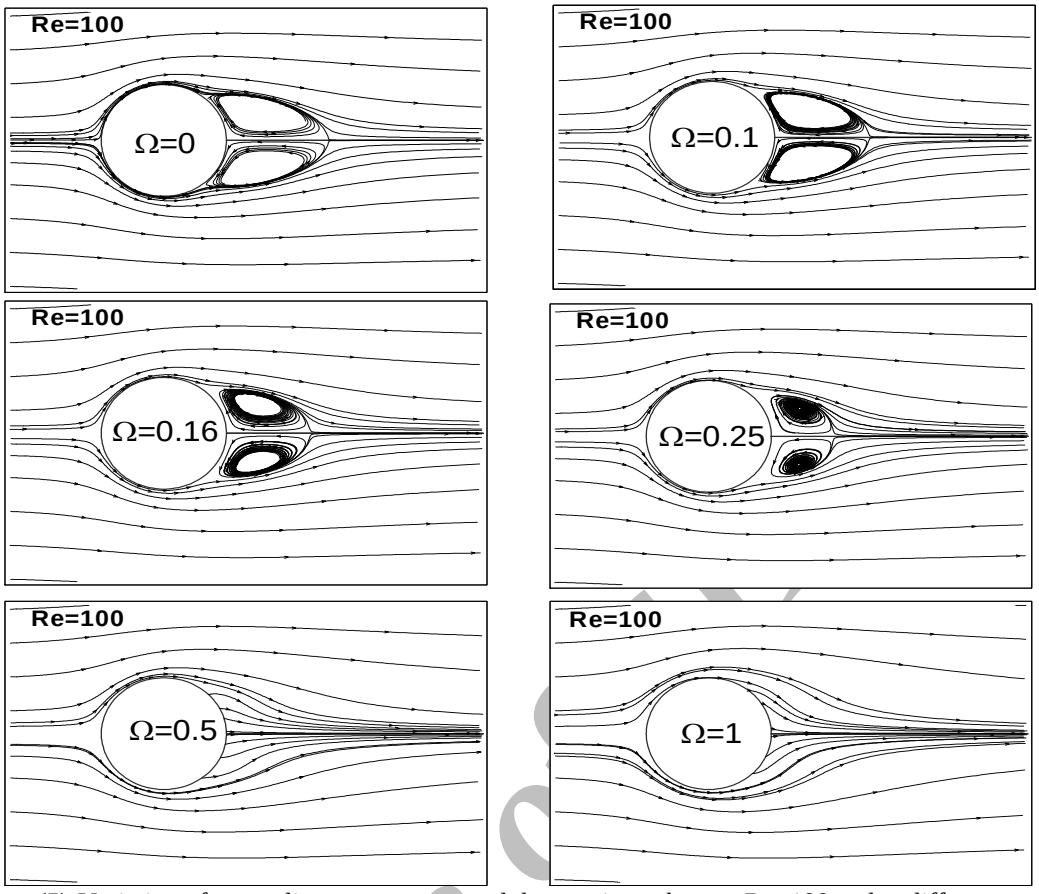

Figure (5): Variation of streamlines patterns around the rotating sphere at Re=100 and at different angular velocity in x-z plane.

As shown in Fig. **6**, increasing Ω_z decreases eddy size and wake length and finally at Ω_z >0.5 this small separation region will be disappeared. As shown in Fig. **6**, the wake length is decreases from L≈0.87*D* at Ω_z =0 to about L≈0.001*D* at Ω_z =0.45. The wake length is defined as the distance from the rear stagnation point to the end of the separated zone along the main flow axis.

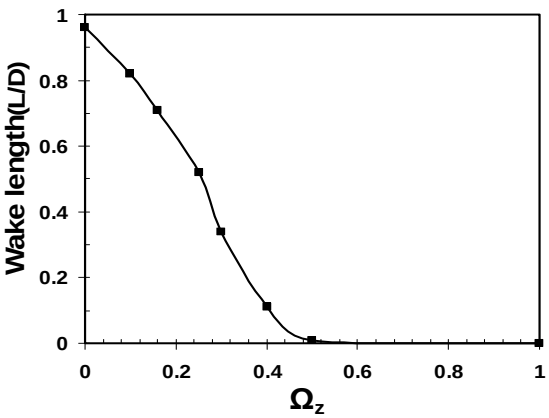

Figure (6): Variation of the wake length with respect to Ω_z in flow around the rotating sphere at Re=100 and different angular velocity in x-z plane.

As it is obtained from Fig. **7**, the separation angle of flow around the rotating sphere in x-z plane decreases with increasing Ω_z and at Ω_z >0.5 there is not shown any separation of flow around the rotating sphere at x-z plane.

The variation of vortisity distribution of flow around the rotating sphere at different rotational speed in x-y plane and Re=100 is shown at Fig. **8**. As shown in Fig. **8** when rotational speed increases, the vortisity lines deviate toward the direction of rotating sphere and the contours of vortisity dispersion is stretched at rear of sphere,(see vortisity line 49.259).

The variation of vortisity distribution of flow around the rotating sphere at different rotational speed in x-z plane and Re=100 is shown at Fig. **9**.

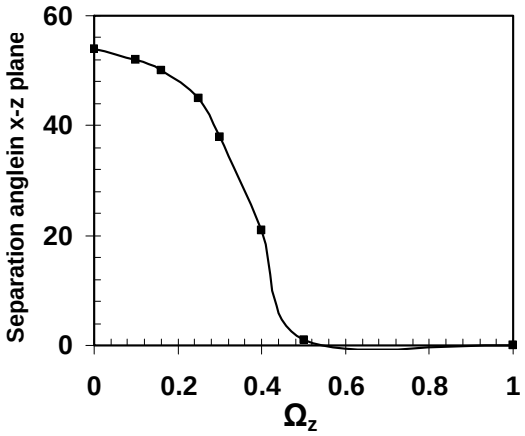

Figure (7): Variation of the separation angle with respect to Ω_z in flow around the rotating sphere at Re=100 and at different angular velocity in x-z plane.

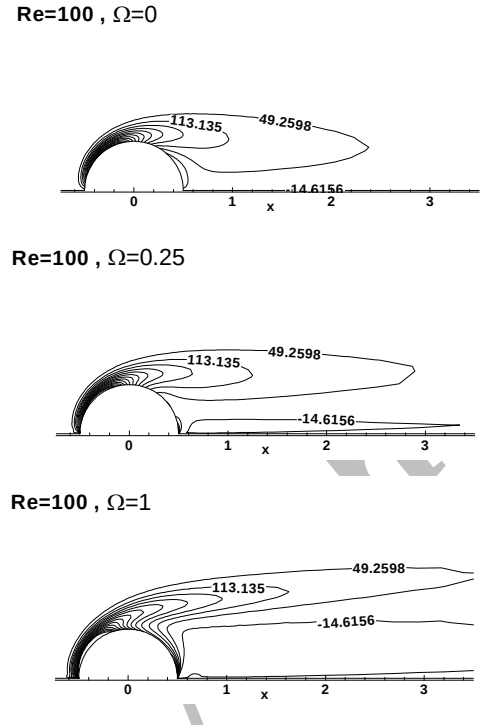

Figure (8): Variation of vortisity patterns around the rotating sphere at Re=100 and different angular velocity in x-y plane.

As shown in Fig. **9** with increasing rotational speed, shear stress effects on the spherical surface increases and this causes that the contours of vortisity dispersion is packed together at rear of sphere,(see vortisity line 48.625).

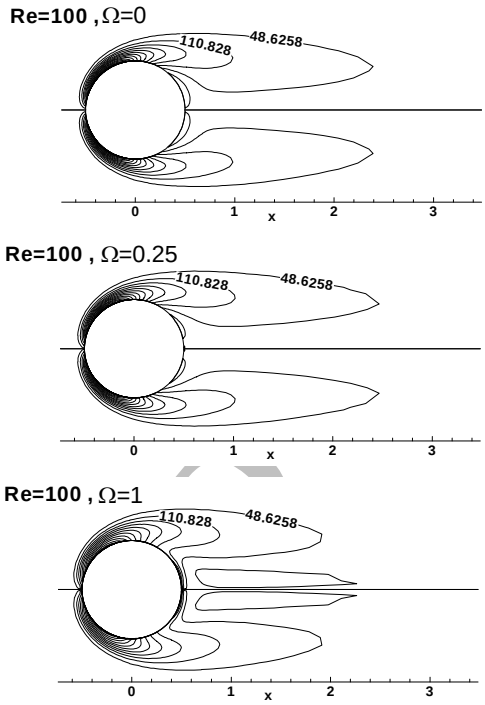

Figure (9): Variation of vortisity patterns around the rotating sphere at Re=100 and different angular velocity in x-z plane.

Variation of surface pressure coefficient (*Cp*) versus dimensionless angle θ at different angular velocity Ω_z in x-y plane and Re=100 is drawn in Fig. **10**. It can be found that the computed results of pressure coefficient at first stagnation point decreases monotonically with increasing angular velocity Ω_z of fluid on the surface.

The variation of the surface pressure (*Cp*) with respect to θ(degree) in flow around the rotating sphere at Re=100 and different angular velocity Ω_z in y-z plane it is shown in Fig. **11**.

As shown in Fig. **11** the surface pressure of rotating sphere at Ω_z =0 is not changed in y-z plane and we can conclude that any lift force (F_{Ly}) is not exerted to the stationary sphere. Increasing Ω_z causes to getting higher surface pressure coefficients (C_{Ly}) in y-z plane and increasing lift force exerted by flow to the rotating spherical particle.

The temporal behavior of the lift coefficient with increasing Ω_z at $Re = 100$ is shown in Fig. **12**.

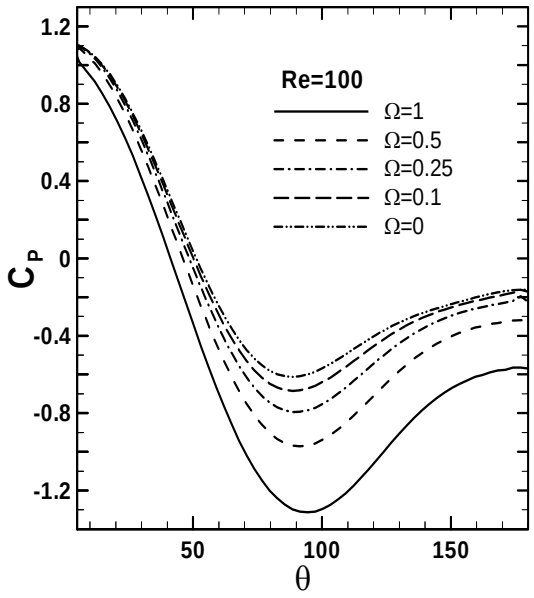

Figure (10): Variation of the surface pressure (*Cp*) with respect to θ(degree) in flow around the rotating sphere at Re=100 and at different angular velocity Ω_z in x-y plane.

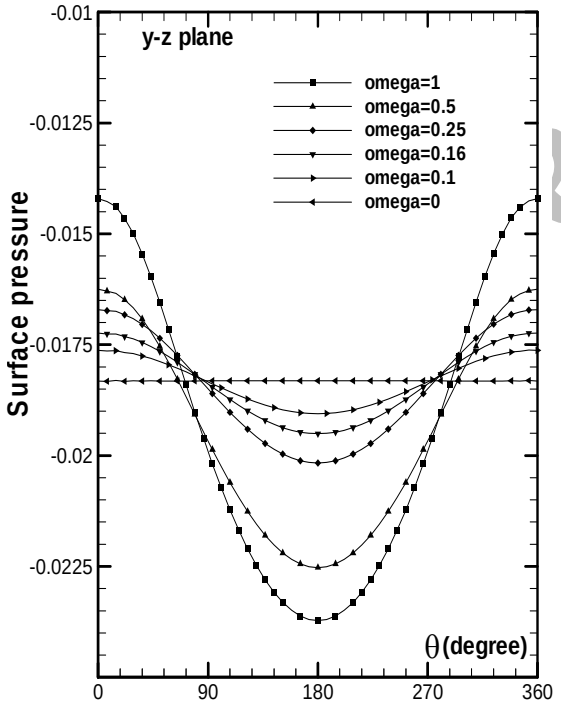

Figure (11): Variation of the surface pressure(*Cp*) with respect to θ(degree) in flow around the rotating sphere at Re=100 and atdifferent angular velocity Ω_z in y-z plane

Increasing angular velocity causes to increase in the lift coefficient (C_L). The effect of angular velocity on lift coefficient is more significant at higher angular velocity numbers such that C_L at Ω_z=1 is 38% larger with respect to Ω_z =0.5, and 78% larger as compared to Ω_z=0.1.

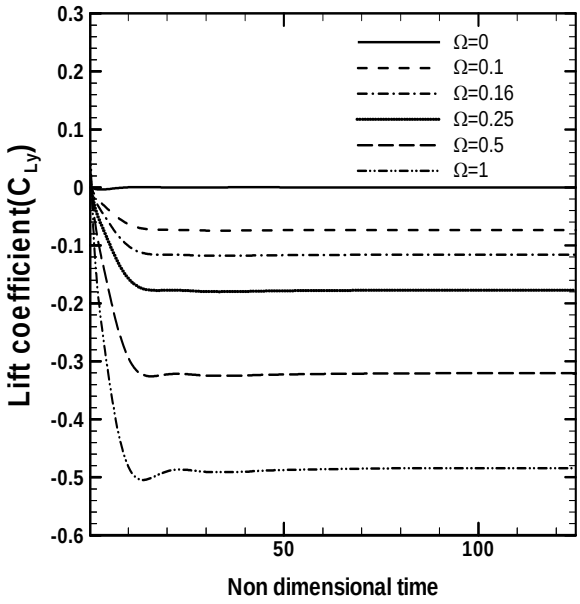

Figure (12): Lift coefficient histories at Re = 100 for different angular velocity Ω_z.

A study of the temporal behavior of the lift coefficient at different angular velocity numbers indicates that lift coefficient, C_L, remains finally steady despite its considerable diminish in initial instants. A reducing behavior of the lift coefficient is observed at very early dimensionless times as shown in Fig. **12**. This is related to the sudden introduction of the rotating sphere into the uniform and steady free stream. Initial lift coefficient behavior is strongly affected by the onset of flow separation and the rate of subsequent wake growth. In an impulsive start, the effects of Ω_z on flow separation and wake growth are immediate whereas the effects of the background flow are delayed (see Fig. **12**) by about 20, which is approximately the transit time of a flow over the spherical particle.

Surface global parameters, such as the drag coefficients, are also influenced by variation of the angular velocity of spherical surface. The drag coefficient increases with increase of Ω_z on the sphere surface and also the drag coefficient behavior depends on the Reynolds number. The temporal behavior of the drag coefficient with increasing Ω_z at $Re = 100$ is shown in Fig. **13**. The effect of Ω_z on C_D at Re=100 is more significant at higher angular velocity such that C_D at Ω_z=1 is 6% larger that that of Ω_z =0.5, and 11.8% larger as compared to Ω_z=0 (stationary sphere).

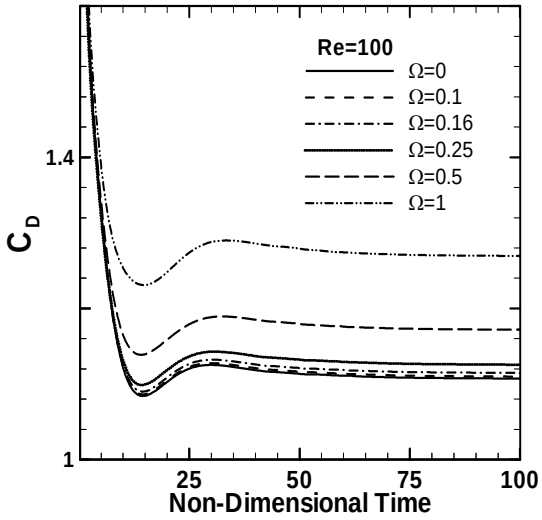

Figure (13): Drag coefficient histories at Re = 100 for different angular velocity Ω_z.

A study of the drag coefficient histories at different angular velocity numbers indicates that drag coefficient (C_D) remains finally steady despite of its considerable decrease in initial instants.

As shown in Fig. **14** the drag coefficient is reduced with increasing Reynolds number and decreasing angular velocity but this variation is not uniform in all ranges of Reynolds numbers. We can investigate this subject with study of drag reduction between special cases of Ω_z=1 and stationary sphere at low and moderate Reynolds numbers regimes**.** As it is shown in Fig.**14** at low Reynolds regime, Re=0.1, computed drag reduction in Ω_z=0 with respect to Ω_z=1is negligible and drag reduction at Re=100 approximately is 16% and this feature shows the angular velocity does not effect on drag coefficients at low Reynolds number regimes and it is important at moderate Reynolds numbers, Re>35.

Figs.**15** shows the comparison of the drag coefficient (C_D) with respect to Reynolds numbers in flow around the rotating sphere at different angular velocity Ω_z. As shown in Fig. **15**, the drag coefficients of rotating spheres at present 3D numerical analysis at different angular velocity Ω_z is compared with other results of flow around of rigid rotating spheres.

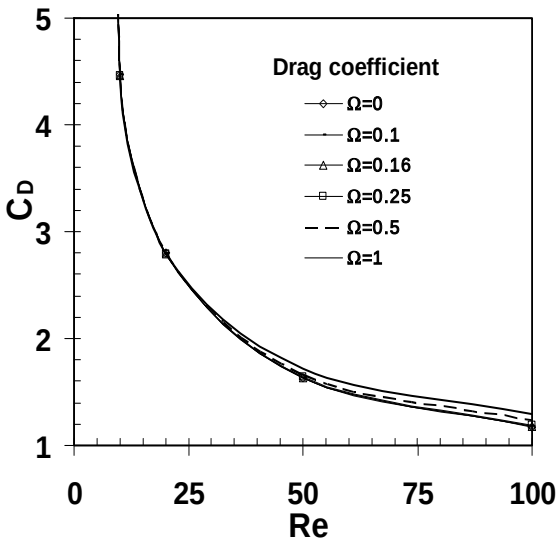

Figure 14: Variation of drag coefficient (C_D) with respect to Reynolds numbers in flowaround the rotating sphere at different angular velocity Ω_z.

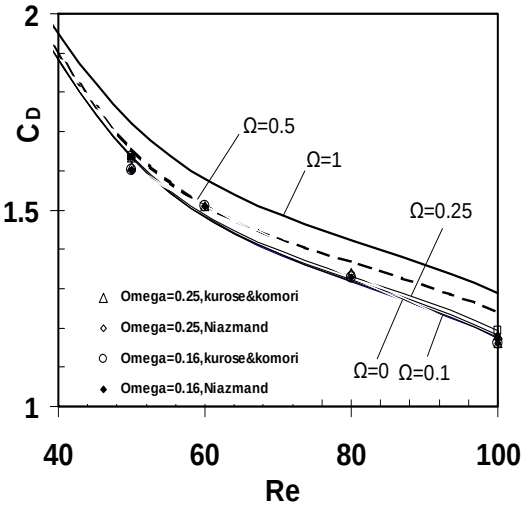

Figure (15): Comparison of the drag coefficient (C_D) versus Reynolds numbers in flow around the rotating sphere at different angular velocity Ω_z.

The computed drag coefficients at present study, the steady-state values of C_D at different Ω_z and 0.1≤Re≤100, have good agreement with other results.

Figure.**16** shows the variation of drag coefficient (C_D) with respect to angular velocity Ω_z in flow around the rotating sphere at moderate Reynolds numbers. As illustrated in Fig. **16**, with increasing angular velocity Ω_z the drag coefficients of rotating spheres is increased at moderate Reynolds, numbers regimes, (Re=50 and 100) but as shown in Figs. **16** and **17** variation of Ω_z does not effects on drag coefficient values at low Reynolds number regimes,(Re=1, 10 and 20).

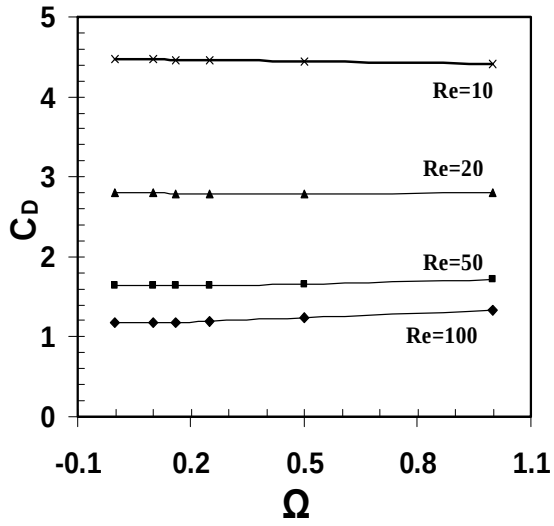

Figure (16): Variation of drag coefficient versus angular velocity Ω_z in flow around the rotating sphere at moderate Reynolds numbers.

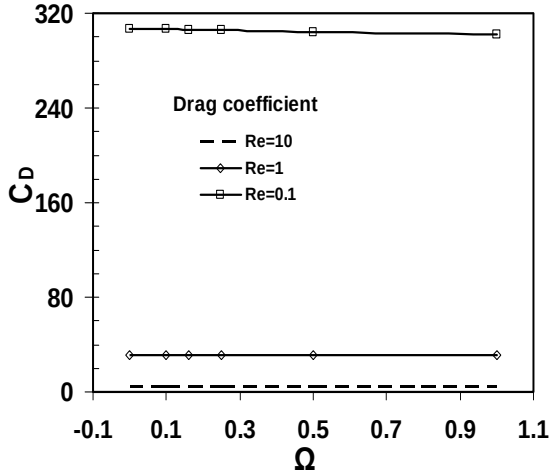

Figure (17): Variation of drag coefficient versus angular velocity in flow around the rotating sphere at low Reynolds numbers.

Figure.**18** shows the comparison of the lift coefficient (C_L) with respect to Reynolds numbers in flow around the rotating sphere at different angular velocity Ω_z with numerical results of references[12] and [15]. As shown in Fig. **19** the steady-state values of C_L at different Ω_z and 0.1≤Re≤100, have good agreement with other results.

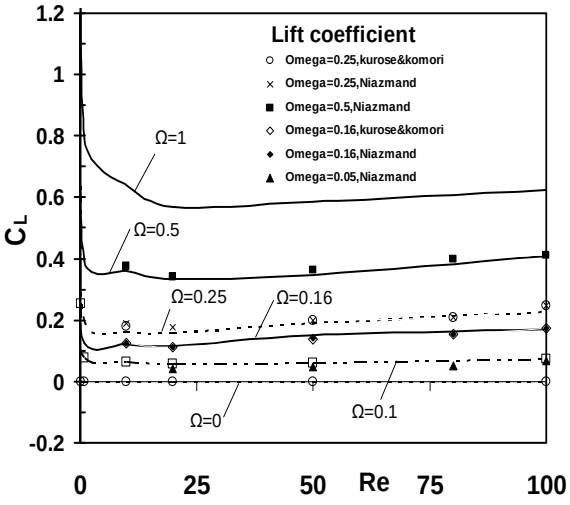

Figure (18): Comparison of the lift coefficient (C_L) with respect to Reynolds numbers in flow around the rotating sphere at different angular velocity Ω_z with numerical results of [12] and [15].

Conclusions

Fluid dynamics characteristics of laminar 3-D flow past an impenetrable rotating suspended spherical particle have been studied with effect of rotation Ω_z <1 in the range 0.1≤Re≤200. The rotation causes the streamlines passing on the rotating sphere not to remain symmetric in x-y plane, but flow patterns remain symmetric at x-z plane. The wake length and separation angle at x-z plane increases with decreasing Ω_z (angular velocity of rotating sphere). Increasing the rotating number, Ω_z is more profound at higher rotation and the present calculations indicate the wake length becoming smaller with increasing Ω_z until it disappears at $\Omega_z \leq 0.5$.

It can be found that the computed results of the pressure coefficient at first stagnation point decreases monotonically with increasing angular velocity Ω_z of fluid on the surface.

A study of the temporal behavior of the lift and drag coefficients at different angular velocities indicates that lift and drag coefficients, C_L, C_D, remain finally steady despite its considerable diminish in initial instants. This is related to the sudden introduction of the rotating sphere into the uniform and steady free stream. Initial behavior is strongly affected by the onset of flow separation and the rate of subsequent wake growth. In an impulsive start, the effects of Ω_z on flow separation and wake growth are immediate whereas the effects of the background flow are delayed by about 20, which is approximately the transit time of a flow over the spherical particle.

At low Reynolds regime, Re=0.1, computed drag reduction in Ω_z=0 with respect to Ω_z=1is negligible and drag reduction at Re=100 approximately is 16% and this feature shows the angular velocity does not effect on drag coefficients at low Reynolds number

regimes and it is important at moderate Reynolds numbers, Re>35.

The effect of Ω_z on C_L is more significant at higher angular velocity numbers such that C_L at Ω_z=1 is 38% larger with respect to Ω_z =0.5, and 78% larger as compared to Ω_z=0.1.

It is shown that with increasing angular velocity Ω_z the drag coefficients of rotating spheres is increased at moderate Reynolds numbers regimes,(Re=50, 100) but variation of Ω_z does not effects on drag coefficient values at low Reynolds number regimes,(Re=1 and 10,20).

It is interesting to say the initial lift coefficient values in z direction at dimensionless time step smaller than 40, which is approximately the transit time of flow over the rotating spherical particle at Ω_z.>0.25 is important and at higher time step these values will be vanished.

References

1. Best, J.L., "The Influence of Particle Rotation on Wake Stability at Particle Reynolds Numbers, $Re_P < 300$ - Implications for Turbulence Modulation in Two-phase Flows", Int. J. Multiphase Flow, 24, pp. 693-720, 1998.
2. Taneda, S. "Experimental Investigation of the Wake Behind a Sphere at Low Reynolds Numbers", J. phys. Soc. Jpn.,11, 1104-8, 1956.
3. Roos, F.W., Willmarth, W.W., "Some Experimental Results on Sphere and Disk Drag", AIAA J., Vol. 9, No. 2, pp. 285-91,1971.
4. Nakamura I. "Steady Wake Behind a Sphere", Physics of Fluids, Vol. 19, No. 1, pp.5-8, 1976.
5. Kim, I. and Pearlstein, A., "Stability of the Flow Past a Sphere", J. Fluid Mech., 211, 73-93, 1990.
6. Natarajan, R. and Acrivos, A., "The Instability of the Steady Flow Past Spheres and Disks", J. Fluid Mech., 254, 323-344, 1993.
7. Magnaudet, J., Rivero, M. and Faber, J. "Accelerated Flows Past a Rigid Sphere or a Spherical Bubble", Part 1. Steady Straining Flow, J. Fluid Mech., Vol. 284, No. 2, pp. 97-135, 1995.
8. Le Clair, B.P., Hammielec, A.E. and Pruppacher, H.E. "A Numerical Study of the Drag of a Sphere at Low and Intermediate Reynolds Numbers", J. Atoms. Sci. , Vol. 27, No. 1, pp. 308, 1970.
9. Brakla, HM., Auchterlonie LJ. "The Magnus or Rubins Effect on Rotating Spheres", J. Fluid Mech., 147, Vol. 147, No. 1, pp.437-47, 1971.
10. Oesterle, B., and Dinh, B., "Experiments on the Lift of a Spinning Sphere in a Range of Intermediate Reynolds Numbers", Experiments in Fluids, Vol. 25, No. 1, pp. 16-22, 1998.
11. Salem, M.B. and Oesterle, B., "A Shear Flow Around a Spinning Sphere: Numerical Study at Moderate Reynolds Numbers", Int. J. Multiphase Flow, Vol. 24, No. 1, pp. 563-585, 1998.
12. Kurose, R. and Komori, S., "Drag and Lift Forces on a Rotating Sphere in a Linear Shear Flow," J. Fluid Mech., Vol. 384, No. 2, pp. 183-206, 1999.
13. Kim, D. and Choi, H., "Laminar Flow Past a Sphere rotating in the Streamwise Direction", J. Fluid Mech., Vol. 461, No. 1, pp. 365-385, 2002.
14. Clift, R., Grace, J.R., and Weber, M. E., "*Bubbles, Drops and Particles*", Academic Press., New York, 1970.
15. Niazmand, H., and Renksizbulut, M., "Transient Three-dimensional Heat Transfer from Rotating Spheres with Surface Blowing", Chem. Eng. Sci., Vol. 58, No. 1, pp. 3535-3554, 2003.
16. Niazmand, H. and Renksizbulut, M. "Surface Effects on Transient Three-dimensional Flows around Rotating Spheres at Moderate Reynolds Numbers," Computers & Fluids, Vol. 32, No.1, pp.1405-1433, 2003.
17. Atefi, Gh., Niazmand, H. and Meigounpoory, M.R., "Numerical Analysis of 3D Flow Past a Stationary Sphere with Slip Condition at Low and Moderate Reynolds Numbers" J. of Dispersion Science and Tech.(In print), Vol. 28, No. 4, pp. 591–602, 2007.
18. Davidson, L. and Farhanieh, B. "A Finite Volume Code Employing Collocate Variable Arrangement and Cartesian Velocity Components for Computing of Fluid Flow and Heat Transfer in Complex Three Dimensional Geometries", Department of Thermo and Fluid Dynamics, Chalmers Univ. of Tech. ,Sweden,1991.
19. Raithby, G.D. , Eckret, E.R.G., Int. J. Heat and Mass Transfer, Vol. 11, No. 2, pp.1233-1252, 1968.
20. Karla, T.R., Uhlherr, P.H.T., 4th Australian. Conf. Hydraulic and Fluid Mechanics, Melborne, 1971
21. Modaress, M.R., Niazmand, H., Mirbozorgi, A., "Three-dimentional Analysis of Flow Past a Solid Sphere ant Low Reynolds Numbers", Esteghlal J., Vol. 2, No. 1, pp.191-205, 2001.